PHYSICAL REVIEW B VOLUME 16, NUMBER 6 15 SEPTEMBER 1977

Theory of spin-disorder Raman scattering in magnetic semiconductors

S. A. Safran,* G. Dresselhaus,† and B. Lax*
Francis Bitter National Magnet Laboratory,‡ Massachusetts Institute of Technology, Cambridge, Massachusetts 02139
(Received 9 May 1977)

Inelastic light scattering from non-zone-center phonons in the magnetic phases of the europium chalcogenides is interpreted in terms of two-spin correlation functions. Calculations of the Raman line shape in paramagnetic EuS are presented in addition to predictions of the temperature dependence of the centroid and integrated intensities of the first-order Raman spectra of all four europium chalcogenides. In the critical region, analytical expressions which relate the temperature dependence of the integrated intensity to the correlation length κ are derived. The calculations make use of a formalism which relates the Raman and conductivity tensors. The symmetry operations of time reversal and spatial inversion are used to show that the scattering tensor arising from a one-phonon–one-spin mechanism is symmetric under the interchange of the incident and scattered photons. The results are compared with existing experiments and the temperature dependence of the characteristic spin frequency in paramagnetic EuS is inferred.

Inelastic light scattering is a valuable tool for studying the elementary excitations of the many-body systems (e.g., electrons, phonons, spins) found in magnetic semiconductors. The dynamics of the phonon system are better understood, at least in principle, than those of the electronic and/or spin systems, the latter being a subject of current investigation.[1-3] Most theories for the behavior of ferromagnetic spin systems have been developed for the Heisenberg ferromagnet[1,4] of which the magnetic semiconductors EuO and EuS are the best known examples. Because the remaining europium chalcogenides, EuSe and EuTe, exhibit a variety of magnetic phases at various values of temperature and external field, these materials, which crystallize in the simple NaCl structure, are useful for the study of the statics and dynamics of spin systems. Recent experimental studies of Raman scattering from phonons in the europium chalcogenides have shown that the Raman spectrum of these materials is magnetic-phase dependent[5-10] and that near resonance the interactions of all three systems—the electrons, phonons, and spins—must be considered in order to understand the Raman spectra.[9,11] In this paper, we interpret the symmetrically polarized, off-resonance Raman scattering from non-zone-center phonons in these materials, in terms of the two-spin correlation functions of EuO, EuS, EuTe, and EuSe.

Previous discussions of light-scattering experiments in magnetic insulators and semiconductors have been concerned with either the long-wavelength components of the two-spin correlation function (one-magnon scattering)[12,13] or with measurements of the four-spin correlation function (two-magnon scattering).[14] The latter quantity is difficult to calculate and to relate simply to the physical properties of the material. On the other hand, the two-spin correlation function, which is related to the response of the spins to a space- and time-varying magnetic field, is simpler to calculate and contains direct information about the magnetic state. The two-spin correlation function is shown to be related to the Raman process by a mechanism involving one spin and one phonon, through spin-orbit coupling.

Section I of this paper contains a review of the quantum-mechanical treatment of low-energy ($\lesssim$200 mV) inelastic light scattering from thermal fluctuations in semiconductors and insulators, in terms of scattering tensors and correlation functions.[13,15] In order to analyze the symmetry of the scattering, the expressions for the scattered intensity are then related to the dielectric response (conductivity) of the electrons (energy gap $\gtrsim$1 eV) which interact with the thermal subsystems such as spins or phonons.

In Sec. II of the paper, we consider the scattering tensor for spin and/or phonon scattering in centrosymmetric magnetic semiconductors. We use the results of Sec. I to show that mechanisms linear in the lattice displacement and in the spin, give rise to a scattering tensor that is symmetric under the interchange of the incident and scattered photon polarizations. Selection rules for several other spin-phonon mechanisms are also discussed.

This formalism is used in Sec. III, where the properties of the symmetrically polarized Raman scattering from non-zone-center phonons are calculated and related to the two-spin correlation function. At high temperatures ($T \gg T_c$), the first-order Raman spectrum is calculated, with results presented for EuS. The temperature dependence

of the broadline integrated intensity and centroid is calculated in the temperature range $T \approx T_c$ for all four europium chalcogenides using mean-field theory. The analytical results show that the integrated intensity is related to the correlation length. In addition, the sharp lines observed in the ordered ($T \ll T_c$) magnetic[9,10] phases of these materials, where wave-vector-independent Raman scattering is symmetry forbidden, are interpreted in terms of the elastic "Bragg" part of the two-spin correlation function, suggesting a method for measuring the sublattice magnetization in antiferromagnets. The relation of these calculations to experiment is discussed in Sec. IV, where the experimental data in EuS are used to infer the temperature dependence of the width of the spectral shape function. In addition, the relation of the present work to the calculations of Suzuki[16] and Sakai and Tachiki[17] is discussed.

I. INELASTIC LIGHT SCATTERING AND KUBO CONDUCTIVITY FORMULA

A. Scattering tensors and correlation functions

The quantum-mechanical treatment of inelastic light scattering from thermal fluctuations utilizes perturbation theory to calculate the transition probability, which is proportional to the scattered intensity. The system Hamiltonian (H_0) is the sum of the Hamiltonians of the noninteracting photons, electrons, and thermal subsystems denoted by A, B, etc. while the perturbation Hamiltonian (H') describes the interactions of the electrons with the radiation and with the thermal subsystems:

$$H = H_0 + H' , \tag{1}$$

$$H_0 = H_{e0} + H_i + H_s + H_A + H_B \cdots , \tag{2}$$

$$H' = H_{ei} + H_{es} + H_{eA} + H_{eB} \cdots . \tag{3}$$

Here, H_{e0} is the Hamiltonian of the electrons, including all electron-electron interactions, but neglecting any couplings to the photons or thermal subsystems. Similarly, the Hamiltonians H_A and H_B describe fully the quantum-mechanical systems A and B. For example, $H_A = H_{\text{spin}}$ might consist of the Heisenberg Hamiltonian and the interaction of the spins with an external magnetic field, while $H_B = H_{\text{lattice}}$ would include the harmonic-oscillator Hamiltonian describing the phonons. H_i and H_s are the Hamiltonians governing the incident and scattered radiation fields, while H_{ei} and H_{es}, included in H', are given by

$$H_{ei(s)} = \int \vec{A}_{i(s)}(\vec{r}) \cdot \vec{j}(\vec{r})\, d\vec{r} , \tag{4}$$

where

$$\vec{j}(\vec{r}) = \sum_{\substack{n \\ \text{electrons}}} (e/mc)\, \vec{P}_n \delta(\vec{r} - \vec{r}_n) . \tag{5}$$

In Eqs. (4) and (5), $\vec{A}(\vec{r})$ is the vector potential of the radiation and $\vec{P}_n$ is the momentum operator of the nth electron. The subscripts i and s stand for the incident and scattered fields, respectively. We have neglected the A^2 term in the electron-radiation interaction, since its contribution to inelastic light scattering has been shown to be small.[18]

The perturbation Hamiltonian H' neglects any radiation–thermal-subsystem interactions, as well as any intersubsystem couplings, and includes only electron-radiation and electron-subsystem terms. The latter interactions are taken to be proportional to a subsystem field operator denoted by $Q_A(\vec{r})$. For example, the spin-orbit interaction couples the electron angular momentum to the localized spins and $Q_A = \vec{S}(\vec{r})$ where

$$\vec{S}(\vec{r}) = \sum_{\kappa l} \vec{S}_{l\kappa} \delta(\vec{r} - \vec{R}(l\kappa)) . \tag{6}$$

Similarly, the electron-phonon interaction is proportional to the lattice displacement operator $Q_B = \vec{U}(\vec{r})$ where

$$U_\alpha(\vec{r}) = \frac{1}{(NM_\kappa)^{1/2}} \sum_{\substack{qj \\ \kappa l}} w_\alpha(\kappa | \vec{q} j) Q(\vec{q} j) \times e^{i\vec{q}\cdot\vec{r}} \delta(\vec{r} - \vec{R}(l\kappa)) . \tag{7}$$

In Eqs. (6) and (7), α labels the vector components of the polarization vector $\vec{w}$, while j labels the phonon branch, l the primitive unit cell, and κ the atom of mass M_κ within the primitive unit cell. The normal coordinate, $Q(\vec{q}j)$, where $\vec{q}$ is the wave vector defined in the first Brillouin zone, can be written as a linear combination of phonon creation and annihilation operators.[19]

Third-order perturbation theory yields the transition probability for the excitation of one subsystem in inelastic light scattering (e.g., one-phonon or one-magnon processes). The scattering cross section, for scattering a photon from a state with energy (momentum) $\hbar\omega_i$ ($\hbar\vec{k}_i$), to a state with energy (momentum) $\hbar\omega_s$ ($\hbar\vec{k}_s$), is proportional to the dynamic structure factor

$$\mathcal{S}(\vec{p}, \omega) = \int \langle Q_B^\dagger(-\vec{p}, 0) Q_B(-\vec{p}, t) \rangle e^{-i\omega t} dt \times |\chi_{isB}(\vec{k}_i - \vec{k}_s, \omega_i, \omega_B)|^2 . \tag{8}$$

The momentum and energy transfer $\vec{p}$ and ω, are defined by

$$\vec{p} = \vec{k}_i - \vec{k}_s \tag{9}$$

and

$$\omega = \omega_i - \omega_s . \tag{10}$$

In the expression for $\mathcal{S}(\vec{p}, \omega)$, $\langle\ \rangle$ is a thermal average, and $Q_B(\vec{p}, t)$ is the Fourier transform of the B-subsystem field operator in the Heisenberg representation, where

$$Q_B(t) = e^{iH_B t} Q_B(0) e^{-iH_B t} . \tag{11}$$

For example, for the lattice displacement operators, the correlation functions are[18]

$$\sum_{\alpha\beta} \langle U_\alpha^\dagger(\vec{k}, 0) U_\beta(-\vec{k}, t)\rangle \propto \sum_j \left(\frac{e^{i\omega_j(\vec{k})t}}{\omega_j(\vec{k})} [n_j(\vec{k}) + 1] + \frac{e^{-i\omega_j(\vec{k})t}}{\omega_j(\vec{k})} n_j(\vec{k}) \right), \tag{12}$$

where $\omega_j(\vec{q})$ is the frequency of a phonon of branch j and wave vector $\vec{q}$, while $n_j(\vec{q})$ is the Bose occupation factor. The tensor χ_{isB} in Eq. (8) consists of a ground-state expectation value (for $kT \ll 1$ eV) of electronic operators with symmetries given by the product of the incident and scattered photon polarization vectors $\vec{\epsilon}_i$ and $\vec{\epsilon}_s$ and the subsystem operator Q_B of wave vector $\vec{p}$. Explicit forms for χ for one-phonon and one-magnon scattering in terms of electronic matrix elements are given by Loudon.[12,20]

Higher-order perturbation expansions for the transition probability yield expressions describing the excitation of two (or more) subsystems. If the interference between the various orders can be neglected (valid if one is weak or in a different frequency range), the dynamic structure factor describing the excitation of subsystems A and B can be written

$$\mathcal{S}(\vec{p}, \omega) = \sum_q \int dt\, e^{-i\omega t} \langle Q_A^\dagger(-\vec{p} + \vec{q}, 0) Q_A(-\vec{p} + \vec{q}, t)\rangle \langle Q_B^\dagger(-\vec{q}, 0) Q_B(-\vec{q}, t)\rangle\, |\chi_{isAB}(\vec{k}_i - \vec{k}_s, \vec{q}, \omega_i, \omega_A, \omega_B)|^2 . \tag{13}$$

Here, we have factored the correlation function in accordance with the neglect of any direct A-B interactions. In the approximation that the subsystem energies can be neglected relative to the photon and electronic energies (valid away from the resonance peaks), the scattering tensor is independent of the state of the subsystems, and involves only the electronic and photon states. The thermal properties of the scattering are then described by the correlations functions, while the symmetry of the scattering as well as its dependence on incident photon energy is given by the scattering tensor.

As an example, we consider the fourth-order perturbation term using the spin-orbit and electron-phonon interactions in H', to obtain a term describing the excitation of both the phonon and spin systems by the radiation coupled to the electrons which are coupled to these thermal subsystems.[17] In the approximation that the spin and phonon energies can be neglected relative to the electronic energies involved, the dynamic structure factor [Eq. (13)] for Stokes scattering, can be written

$$\mathcal{S}(\vec{p}, \omega) = \sum_{\substack{jq \\ \sigma\sigma'}} [n_j(\vec{q}) + 1] \int dt\, e^{-i[\omega - \omega_j(\vec{q})]t} \langle S_\sigma(\vec{p} + \vec{q}, 0) S_{\sigma'}(-\vec{p} - \vec{q}, t)\rangle [\chi_{isj\sigma}^*(\vec{p}, \vec{q}, \omega_i) \chi_{isj\sigma'}(\vec{p}, \vec{q}, \omega_i)]/\omega_j(\vec{q}) . \tag{14}$$

Here, the first factor comes from the phonon creation part of the phonon correlation function of Eq. (12). $S_\sigma(\vec{k}, t)$ is the Fourier transform of the localized spin operator ($\sigma = x, y, z$) of Eq. (6) in the Heisenberg representation. The scattering tensor transforms as the direct product of the polar vectors describing the incident and scattered electric fields, the phonon polarization vector, and an axial vector in the σ direction. Although similar expressions can be written for one-phonon–two-spin processes, using a different physical mechanism,[16,17] the discussion of Sec. II will show that the one-phonon–one-spin and the one-phonon–two-spin mechanisms can be experimentally identified by their polarization selection rules. Hence, the two processes do not interfere in certain scattering geometries, enabling the direct comparison of the one-phonon–one-spin calculation with experiment.

B. Symmetry of the conductivity tensor

While the explicit expressions for the scattering tensors derived from the perturbation Hamiltonians can be used to analyze the symmetry of the scattering, it is physically meaningful to obtain these properties by relating the tensors to other, better known, properties of the electronic system such as the conductivity. By calculating the scattering intensity for elastic scattering, where the thermal subsystems are treated like classical, rigid potentials, one can identify the inelastic scattering tensors with terms in the expansion of the conductivity given by the Kubo formula.[21] The calculation of the elastic scattering amplitude proceeds by neglecting the time dependence of the subsystem operators since the subsystem energies are much smaller than both the electronic energy gaps in insulators and semiconductors and the optical

photon energies. The system Hamiltonian is then taken to be

$$H_0 = H_e + H_i + H_s , \tag{15}$$

where H_e includes the interaction of the electrons with the "external fields" (thermal subsystems) so that

$$H_e = H_{e0} + H_{eA} + H_{eB} + \cdots . \tag{16}$$

The interaction Hamiltonian H' consists of only the electron-radiation interactions $H_{ei} + H_{es}$, all other interactions having been included in H_e. Since the thermal subsystems are assumed to be time independent, low-energy scattering, where the electrons remain in their ground state, is elastic. The error involved in this approximation is of the order of (see the Appendix)

$$\omega_{\text{subsystem}}/\omega_{\text{electron}} \simeq \omega_{\text{subsystem}}/\omega_{\text{photon}} \tag{17}$$

and is of the order of 0.01 for typical materials. The changes in the photon polarization and momentum are due to the fact that the electronic system has lower symmetry when the electron-field (subsystem) interactions are included in H_e. The elastic scattering amplitude is given by the conductivity tensor

$$\sigma_{is}(\vec{k}_i, -\vec{k}_s, \omega_i) = \frac{1}{\hbar\omega}\int_0^\infty e^{i\omega_i t}\langle[j_i(\vec{k}_i, 0), j_s(-\vec{k}_s, t)]\rangle\, dt \equiv \int_0^\infty e^{i\omega_i t}\sigma_{is}(\vec{k}_i, -\vec{k}_s, t)\, dt . \tag{18}$$

The conductivity tensor is related to the dielectric constant by $\epsilon_{is} = \epsilon_{is}^{(0)} + (4\pi i/\omega)\sigma_{is}$. In Eq. (18), $j_\alpha(\vec{k}, t)$ is the α component of the Fourier transform of the current operator for the electronic system in Heisenberg picture, including all electron–"external field" (subsystem) interactions.[22] (We have neglected the A^2 term in H_{ei} and H_{es}.) The square brackets signify a commutator, while the expectation value, which is only over the electron coordinates (the subsystems are treated like classical fields), is equivalent to a ground-state expectation value for $k_B T \ll 1$ eV. The conductivity tensor of Eq. (18) represents the response at wave vector $\vec{k}_s$ and frequency ω_i of the electrons (including all interactions with "external fields" $A, B \ldots$) to an incident electric field with polarization $\vec{\epsilon}_i$, wave vector $\vec{k}_i$, and frequency ω_i in the approximation that the subsystem energies are neglected. By manipulation of the commutator in Eq. (18) one can show that the symmetry of the conductivity tensor under the interchange of the incident and scattered photons is determined by the relation

$$\sigma^*_{is}(\vec{k}_i, -\vec{k}_s, t) = \sigma_{si}(\vec{k}_s, -\vec{k}_i, -t) . \tag{19}$$

II. SYMMETRY OF SPIN-PHONON SCATTERING

A. Scattering and conductivity tensors

In the approximation that the subsystem energies can be neglected, the inelastic scattering tensors of Eqs. (8) and (13) can be identified with terms in the perturbation expansion of the conductivity that are linear in Q_B and $Q_A Q_B$, respectively. The conductivity tensor, as defined, is the linear response to the radiation field, but is exact to all orders in the electron-subsystem couplings in the approximation that the subsystem energies are neglected. Consequently, σ_{is} can be expanded using perturbation theory to evaluate the commutator of Eq. (18). However, if the exact matrix elements are unknown, one can still write a phenomenological expansion of σ_{is} in powers of the field operators Q_A, etc. Since the terms of this expansion are written as the products of external fields and tensors (which can be evaluated as phenomenological representations of the matrix elements) which depend only on the state of the bare [H_{e0} of Eq. (2)] electronic system, Eq. (19) is applicable to each term in the expansion with the constraint that the electron–thermal-subsystem interaction Hamiltonian be Hermitian.

A simple example of the use of Eq. (19) to determine the symmetry of the scattering under the interchange of the incident and scattered polarizations is its application to phonon scattering. In the dipole ($\vec{k}_i = \vec{k}_s = 0$) approximation, the term in the conductivity tensor proportional to $\vec{U}(\vec{r})$ is

$$\sigma_{is}(t) = \sum_{j\alpha l\kappa} \omega_\alpha(\kappa|0j)Q(0j)\chi_{isj}(\vec{R}(l\kappa), t) = \sum_j Q(0j)\chi_{isj}(0, t) , \tag{20}$$

where the quantities are defined in Sec. I. The tensor $\chi_{isj}(0, t)$ corresponds to the temporal Fourier transform of the Raman tensor in the treatment of inelastic scattering given in Eq. (8). Since the phonon normal coordinate and polarization vector satisfy[19]

$$Q(\vec{k}j) = Q^*(-\vec{k}j)$$

and

$$w_\alpha(\kappa|\vec{k}j) = w^*_\alpha(\kappa|-\vec{k}j) , \tag{21}$$

and since the phonon polarization vector for $\vec{k} = 0$ is invariant under time-reversal symmetry, one sees that the application of Eq. (19) to this term in the expansion implies that the one-phonon Raman tensor is symmetric under the interchange of the incident and scattered polarizations (symmetrically polarized). Using the antisymmetry of the spin operator under time reversal, one can similarly prove that one-magnon Raman scattering is

antisymmetric under the interchange of the incident and scattered polarizations. These selection rules have been predicted theoretically[12,20] and verified experimentally.[12] They are approximate selection rules that are valid away from sharp resonance peaks in accordance with the assumptions necessary to relate the inelastic scattering tensor to the conductivity.

B. Application to spin-phonon scattering

Another implication of Eq. (19) is the imposition of symmetry requirements on spin-phonon scattering in materials with one magnetic ion per unit cell and with a center of inversion at each atomic site. In particular, in such materials, in the limit $\vec{k}_i = \vec{k}_s = 0$, mechanisms linear or quadratic in both the lattice displacements and spins yield symmetric scattering tensors, while those linear in the spin (lattice displacement) and quadratic in the lattice displacement (spin) are antisymmetric under the interchange of the incident and scattered polarizations. Wave-vector-dependent processes, linear in $\vec{p} = \vec{k}_i - \vec{k}_s$, have the opposite selection rules, while spin and wave-vector-independent two-phonon scattering is symmetric. These selection rules, which are related to those given by Portigal and Burstein[23] for magnetospatial effects, enable the separation of one-phonon–one-spin spectra from the one-phonon–two-spin spectra by their polarization.

As an example of the utility of Eq. (19) in determining the symmetry of the scattering, we consider the derivation of the symmetry of the one-phonon–one-spin terms in the expansion of the conductivity in the dipole approximation. Since the properties of the scattering tensor are independent of the state of the spin or phonon systems, we consider a term in the expansion of σ_{is}, involving the interaction of the electrons with a phonon "field" of wave vector $\vec{q}_0$ and branch j and with a spin "field" of wave vector $-\vec{q}_0$ (translational symmetry dictates that the phonon and spin wave vectors be equal and opposite). For this case

$$\sigma_{is}(t) = S_\sigma(\vec{q}_0) Q(-\vec{q}_0 j) \chi_{isj\sigma}(\vec{q}_0, t) + S_\sigma(-\vec{q}_0) Q(\vec{q}_0 j) \chi_{isj\sigma}(-\vec{q}_0, t) , \quad (22)$$

where we have included "waves" of both $\pm\vec{q}_0$ in accordance with the requirement of the Hermiticity of the interaction Hamiltonians (equivalent to requiring the spin and phonon fields be real). In Eq. (22), $\chi_{isj\sigma}(\vec{q}_0, t)$ can be identified with the Fourier transform of the scattering tensor of Eq. (14) for the one-phonon–one-spin process, in the approximation that the spin and phonon energies are neglected. The scattering tensor can then be written

$$\chi_{isj\sigma}(\vec{q}, t) = \sum_{ll'\kappa\alpha} \exp\{i\vec{q}\cdot[\vec{R}(l'0) - \vec{R}(l\kappa)]\} \times w_\alpha(\kappa|-\vec{q}\,j) \chi_{is\alpha\sigma}(\vec{R}(l'0) - \vec{R}(l\kappa), t) . \quad (23)$$

In this expression w_α is the α component of the polarization vector $\vec{w}$ defined above, while l and l' label the primitive unit cell, and κ the type of atom within it, with the magnetic atom at $\kappa = 0$. Maradudin *et al.*[19] prove that for crystals with every ion at a center of inversion

$$w_\alpha(\kappa|\vec{q}\,j) = w_\alpha(\kappa|-\vec{q}\,j) . \quad (24)$$

Using this property, Eq. (21), and the property that

$$S_\sigma(\vec{q}) = S^*_\sigma(-\vec{q}) , \quad (25)$$

one can show that the invariance of the scattering tensor under inversion symmetry and the imposition of Eq. (19) requires

$$\chi_{isj\sigma} = \chi_{sij\sigma} , \quad (26)$$

demonstrating the symmetry of the one-phonon–one-spin scattering tensor. A similar proof can be applied to the other cases mentioned above to derive the symmetries summarized in Table I. These results can also be derived from explicit considerations of the matrix elements as shown in the Appendix.

III. APPLICATION TO RAMAN SCATTERING IN THE EUROPIUM CHALCOGENIDES

A. Evaluation of dynamic structure factor

Symmetric ($\vec{\epsilon}_i \| \vec{\epsilon}_s$) spin-dependent "broadline" scattering has been observed in the NaCl-structure europium chalcogenides where first-order wave-vector-independent Raman scattering is symmetry forbidden.[5-10] Since wave-vector-dependent ($\vec{k}_i, \vec{k}_s \neq 0$) LO-phonon scattering depends on reso-

TABLE I. Symmetry of inelastic light scattering in centrosymmetric magnetic insulators and semiconductors in dipole approximation.[a]

	Single excitation	one-spin	two-spin
Single excitation		A	S
1 phonon	S	S	A
2 phonon	S	A	S

S, symmetric polarization $\chi_{is} = \chi_{si}$

A, antisymmetric polarization $\chi_{is} = -\chi_{si}$, $\chi_{is} = 0$ if $i = s$

[a] Wave-vector-dependent scattering, linear in $\vec{p} = \vec{k}_i - \vec{k}_s$ has opposite selection rules for spin-phonon processes. For the range of validity of these selection rules, see the Appendix.

nant enhancement,[11] it can be separated from the broadline process, involving the entire LO branch, by tuning the incident frequency off resonance. The wave-vector-independent symmetrically polarized broadline scattering can be analyzed using Eq. (14), while the antisymmetrically polarized scattering requires the use of the one-phonon–two-spin mechanism and the evaluation of a four-spin correlation function. For Stokes scattering from the LO branch in the dipole approximation, the dynamic structure factor for wave-vector-independent one-phonon–one-spin scattering is

$$\mathcal{S}(0,\omega)=\sum_{\substack{\vec{q}\\ \sigma,\sigma'\\ j=\mathrm{LO}}}\int dt\,\exp\{-i[\omega-\omega_j(\vec{q})]t\}\times\langle S_\sigma(-\vec{q},0)S_{\sigma'}(\vec{q},t)\rangle\times[n(\omega_j(\vec{q}))+1]f_{isj\sigma\sigma'}(\vec{q},\omega_i)\,. \tag{27}$$

In Eq. (27), f is a form factor given by the quotient of the square of the Raman tensor and the phonon frequency where

$$f_{isj\sigma\sigma}=|\chi_{isj\sigma}(\vec{q},\omega_i)|^2/\omega_j(\vec{q})\,. \tag{28}$$

The temperature dependence of the scattering at low temperatures where $n(\omega_{\mathrm{LO}}(\vec{q}))\simeq 0$, is thus governed by the Fourier transform of the spin-spin correlation function.

To evaluate Eq. (27), we use a Fourier expansion for the Raman tensors and phonon frequency spectrum,[24] treating the LO branch as nondegenerate. This approximation, valid away from the Γ point ($\vec{q}_\Gamma=0$) in the NaCl structure, is justified since inversion symmetry dicatates that the Raman tensor of Eq. (27) goes to zero as $\vec{q}$ goes to zero. In addition, we assume that the LO polarization vectors transform as components of polar vectors in the direction of $\vec{q}$. Using these approximations, we find that the Raman tensor for scattering with the incident and scattered radiation polarized along the crystal axis ($i=s=x,y,z$) is given by

$$\chi_{zzj\sigma}(\vec{q},\omega_i)=(1/q)[(\alpha q_y\delta_{\sigma,z}+\beta q_z\delta_{\sigma,y})\sin\tfrac{1}{2}q_x a-(\beta q_z\delta_{\sigma,x}+\alpha q_x\delta_{\sigma,z})\sin\tfrac{1}{2}q_y a+\gamma(q_x\delta_{\sigma,y}-q_y\delta_{\sigma,x})\sin\tfrac{1}{2}q_z a]\,. \tag{29a}$$

Similarly, the tensor for symmetric xy polarization ($\epsilon_i^x\epsilon_s^y+\epsilon_i^y\epsilon_s^x$) is

$$\chi_{xyj\sigma}(\vec{q},\omega_i)=(1/q)[(Aq_x\delta_{\sigma,z}+Bq_z\delta_{\sigma,x})\sin\tfrac{1}{2}q_x a-(Aq_y\delta_{\sigma,z}+Bq_z\delta_{\sigma,y})\sin\tfrac{1}{2}q_y a+C(q_x\delta_{\sigma,x}-q_y\delta_{\sigma,y})\sin\tfrac{1}{2}q_z a]\,. \tag{29b}$$

Here, a is the cubic-lattice constant while A, B, C, α, β, and γ are constants which depend on the electronic matrix elements and energies, and ω_i. The expansion takes as its origin the magnetic ion and is truncated at the nearest neighbor—the chalcogenide ion. Symmetry dictates that the zeroth-order term vanishes, implying that the first nonvanishing contribution to $\vec{q}$-dependent phonon scattering in these materials is due to the spin-electron-phonon couplings involving the europium ion and its nearest neighbor. The standard Fourier expansion for the phonon frequency, calculated with the EuX molecule at the origin and truncated at the first lattice vector, yields

$$\omega_{\mathrm{LO}}^2(\vec{q})=\omega^2(L)+\tfrac{1}{3}[\omega^2(\Gamma)-\omega^2(L)]\times[\cos\tfrac{1}{2}q_x a\cos\tfrac{1}{2}q_y a+\cos\tfrac{1}{2}q_x a\cos\tfrac{1}{2}q_z a+\cos\tfrac{1}{2}q_z a\cos\tfrac{1}{2}q_y a]\,. \tag{30}$$

The constants in this expression are evaluated from the experimental data of Ref. 25 for the Γ point LO frequency. The L point [$a\vec{q}_L=\pi(1,1,1)$] has been assigned to the peak of the broadline,[8] consistent with both our calculations and the experimental evidence of Ref. 8. The parameters used in our calculations are listed in Table II. From Eq. (29a), it is evident that for zz polarization, the Raman tensor vanished along the [100] and [110] axes, while the contributions from the [111], [011], and [101] axes result in the same combination of the constants, $\beta+\alpha$. For xy polarization, there is a contribution from the [100] and [010] directions in addition to the ones contributing to the zz spectrum, but with different constants. The sum over $\vec{q}$ is calculated by the numerical method of Gilat and Bohlin.[26]

In addition to the Raman tensor, the scattering intensity depends on the two-spin correlation function. In general, the two-spin correlation function can be written[4]

$$\langle S_\sigma(-\vec{q},0)S_{\sigma'}(\vec{q},\omega)\rangle=\frac{S(S+1)}{3}\frac{\hbar\omega\beta}{1-e^{-\hbar\omega\beta}}\frac{\chi_{\sigma\sigma'}(\vec{q})}{\chi_0}F_{\sigma\sigma'}(\vec{q},\omega)+\frac{\delta(\omega)}{N}\langle S_{\sigma'}(\vec{q})\rangle\langle S_\sigma(-\vec{q})\rangle\,. \tag{31}$$

TABLE II. Experimental parameters for spin and phonon systems in europium chalcogenides.

	$\omega(\Gamma)$[a]	$\omega(L)$[a]	J_1[b]	J_2[b]
EuO	435	411	0.606	0.119
EuS	267	240	0.236	−0.118
EuSe	182	153	0.167	−0.158
EuTe	142	131[c]	0.100	−0.213

[a] $\omega(\vec{q})$ is LO phonon frequency in cm^{-1}, see Ref. 25.
[b] J_1 and J_2 are nearest-neighbor and next-nearest-neighbor exchanges in °K, see Ref. 1.
[c] See Ref. 38.

The first term of Eq. (31) represents the contribution to the inelastic, diffuse scattering due to short-range order, while the second term of Eq. (31), proportional to the square of the sublattice magnetization, is a measure of the long-range order in the temperature region below T_c, and is hence termed the magnetic Bragg scattering. In Eq. (31), S is the dimensionless magnitude of the z component of the spin, and $\beta = 1/k_B T$. The second factor in the first term of this equation is a detailed balance factor, which is approximately equal to one at sufficiently high temperatures ($T \gg \hbar\omega/k_B$), while $\chi(\vec{q})/\chi_0$ is the ratio of the wave-vector-dependent susceptibility to the Curie susceptibility, and is a function of the temperature and the exchange constants. For Heisenberg ferromagnets near the critical temperature T_c, mean-field theory yields ($T > T_c$)

$$\frac{\chi_{\sigma\sigma'}(\vec{q})}{\chi_0} = \delta_{\sigma\sigma'}\left(\frac{T - T_c}{T_c} + \frac{J(0) - J(\vec{q})}{J(0)}\right)^{-1} . \tag{32}$$

Here $J(\vec{q})$ is the $\vec{q}$th Fourier component of the exchange between a spin located at the origin, and one located at a distance $\vec{R}$. The final factor in the first term of Eq. (31) is the spectral shape function, which describes the dynamic response of the spin system to a time-varying magnetic field. The temporal Fourier transform of $F(\vec{q},\omega)$ is the ratio of the time-dependent relaxation function[4] to its value at $t = 0$, which leads directly to the identity,

$$\int_{-\infty}^{\infty} F(\vec{q}, \omega)\, d\omega = 1 . \tag{33}$$

At low temperatures this function, which gives the neutron scattering line shape, consists of two peaks centered at $\omega \pm \omega_m(\vec{q})$ corresponding to the creation and destruction of magnons of wave vector $\vec{q}$ and energy $\hbar\omega_m(\vec{q})$.[4]

Using these results for the spin-spin correlation function, and Eqs. (29a) and (30) for the form factor and the phonon frequency, we have investigated the one-phonon–one-spin, symmetrically polarized contribution to inelastic light scattering in the europium chalcogenides. We present the results of our calculations for the high- ($T \gg T_c$), intermediate- ($T \approx T_c$), and low- ($T \ll T_c$) temperature regimes, where T_c is the transition temperature for all the magnetic phases.

B. Spin-dependent Raman spectra

1. High temperatures ($T \gg T_c$)

At high temperatures ($T \gg T_c$), the spins are spatially uncorrelated and there is no ordering to distinguish the longitudinal and transverse components of $\chi_{\sigma\sigma'}(\vec{q})$. Consequently $\chi_{\sigma\sigma'}(\vec{q})/\chi_0$ of Eq. (32) is approximately equal to $\delta_{\sigma\sigma'}$. The temperature dependence of the scattering is governed by the phonon population factor, with the spectrum being composed of the sum of contributions from LO phonons from the entire zone. Each contribution is weighted by the product of the form factor and the phonon population factor, each weighing the zone-boundary phonons heavily. The dynamic structure factor for scattering from the LO branch with zz polarization (off resonance) is

$$S(0,\omega) = \sum_{\substack{\vec{q},\sigma \\ j=\mathrm{LO}}} f_{zzj\sigma\sigma}(\vec{q}, \omega_i)[n(\omega_j(\vec{q})) + 1] \times F(\vec{q}, \omega - \omega_j(\vec{q})) . \tag{34}$$

At these high temperatures the system can be thought of as being spatially amorphous, allowing scattering from all $\vec{q}$ vectors in the zone. Although the statics of the spins play no role in this temperature regime (all $\vec{q}$ vectors are weighted equally by the susceptibility as $T \to \infty$), the nature of the spin dynamics does influence the spectrum through the spectral shape function $F(\vec{q}, \omega - \omega_j(\vec{q}))$. This function is not a δ function in $\omega - \omega_j(\vec{q})$ even in the limit of infinite temperatures, due to the nonuniform temporal response of the spins to a time-varying magnetic field, even at $T \to \infty$. Although exact analytical forms of $F(\vec{q}, \omega)$ are unknown even at high temperatures, a useful first approximation for ferromagnets (especially valid at large wave vector) is the Gaussian[27]

$$F(\vec{q}, \omega) \simeq \frac{1}{[2\pi F^{(2)}(\vec{q})]^{1/2}} \exp\left(-\frac{\omega^2}{2F^{(2)}(\vec{q})}\right) . \tag{35}$$

In Eq. (35), $F^{(2)}(\vec{q})$ is the second moment of the spectral shape function and is given by[27]

$$F^{(2)}(\vec{q}) = \tfrac{8}{3} S(S+1) \sum_{R} [J(\vec{R})]^2 (1 - e^{i\vec{q}\cdot\vec{R}}) . \tag{36}$$

Figure 1 shows the results of a numerical inte-

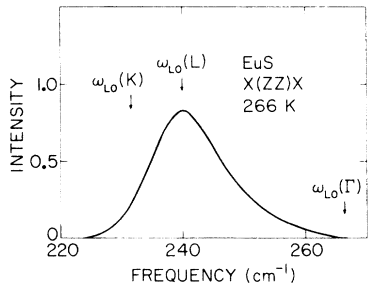

FIG. 1. Raman line shape for zz-polarized, one-spin–one-phonon mechanism in the paramagnetic phase of EuS at 266 K. The broadening of each contribution is due only to the interactions with the dynamic spin system, any anharmonic phonon broadening has been neglected.

gration of Eq. (34) (with $\alpha=0$, $\beta=\gamma=1$) using the method described above for EuS at $16T_c \simeq 266$ K. The high-temperature broadline is peaked at $\langle\omega_{LO}\rangle \approx 240\ \mathrm{cm}^{-1}$, corresponding to the L-point LO-phonon frequency where the Raman tensor is a maximum. The width of each contribution is calculated using Eqs. (35) and (36) for the spectral shape function. Thus, even neglecting broadening due to finite phonon lifetimes (resulting from anharmonic decay[28]), the contribution from each phonon is broadened due to dynamic spin disorder. Calculation of the symmetric xy polarized spectrum yields lines that are approximately the same as the zz polarized spectra.

2. Critical region ($T \approx T_c$)

At intermediate temperatures, $T \approx T_c$, but $T \ll \hbar\omega_{LO}/k_B$, the phonon population factor is temperature independent. The temperature dependence of the spectrum is determined by the $\vec{q}$-space average of the dynamic spin-spin correlation function, weighted by the form factor f.

Since analytic expressions for $F(\vec{q},\omega)$ in the full range of $\vec{q}$ and T are unknown at this time, we have chosen to calculate the moments of $\mathcal{S}(0,\omega)$ which depend only on the static response of the spins through $\chi_{\sigma\sigma}(\vec{q})/\chi_0$. The zeroth moment of $\mathcal{S}(0,\omega)$ gives the integrated intensity $I(T)$, while the first moment yields the centroid of the spectrum, $\langle\omega\rangle$, which is roughly related to the peak intensity. We therefore define

$$I(T,\vec{q}) = \sum_{\substack{O \\ j=LO}} f_{isj\sigma\sigma}(\vec{q},\omega_i)\frac{\chi_{\sigma\sigma}(\vec{q})}{\chi_0}\frac{S(S+1)}{3} \tag{37}$$

so that the integrated intensity is given by

$$I(T) = \sum_{\vec{q}} I(T,\vec{q}) . \tag{38}$$

The centroid of the spectrum is similarly given by

$$\langle\omega_j\rangle_T = \frac{1}{I(T)}\sum_{\vec{q}}[\omega_j(\vec{q})I(T,\vec{q})] . \tag{39}$$

We have evaluated Eqs. (38) and (39) for the integrated intensity and centroid of the spectrum due to zz-polarized, one-LO-phonon–one-spin scattering in the europium chalcogenides using a small wave-vector expansion for the form factor of Eq. (28). Using mean-field theory, the susceptibility is rewritten in the form

$$\frac{\chi(\vec{q})}{\chi_0} = \frac{(T/T_c)\kappa_0^2}{\kappa^2+\kappa_0^2 g(\vec{q})} , \quad T > T_c , \tag{40}$$

where, for the fcc ferromagnets EuO and EuS,

$$g(\vec{q}) = [J(0)-J(\vec{q})]/J(0) , \tag{41}$$

$$(a\kappa_0)^2 = (12J_1+6J_2)/(J_1+J_2) . \tag{42}$$

Here J_1 and J_2 are the first- and second-nearest-neighbor exchanges, and $J(\vec{q}) = J_1(\vec{q})+J_2(\vec{q})$. For the two sublattice antiferromagnets, with spins in (111) planes aligned, as in EuTe and EuSe (see Table III), the susceptibility $\chi(\vec{k})$ is defined in terms of $\vec{k} = \vec{q}_L - \vec{q}$. In addition, for these systems, in an angle average,

$$(a\kappa_0)^2 = 6 . \tag{43}$$

In the expressions for the susceptibility, κ is the inverse correlation length and is a measure of the distance over which spins are correlated. In general, the inverse correlation length is determined by

$$\kappa^2 = \kappa_0^2\left(\frac{T-T_c}{T_c}\right)^{2\nu} , \quad T > T_c . \tag{44}$$

Mean-field theory yields the exponent $\nu = \frac{1}{2}$, while recent experiments[1] indicate that $\nu \simeq 0.7$ for the three-dimensional Heisenberg model near T_c, in good agreement with renormalization-group calculations for ν.

TABLE III. Spin ordering and Raman-active sharpline (Bragg) phonons in europium chalcogenides (single-spin mechanism). $\vec{q}_0$ is the wave vector describing magnetic ordering where $\langle S(\vec{q}_0)\rangle$ is nonzero below T_c or T_N.

Material	Order			Phonons
EuO	Ferromagnetic	$T_c = 69.3$ K	$\vec{q}_0 = 0$	LO[a](Γ), TO[a](Γ)
EuS	Ferromagnetic	$T_c = 16.6$ K	$\vec{q}_0 = 0$	LO[a](Γ), TO[a](Γ)
EuSe	Four-sublattice	$T_N = 4.6$ K	$\vec{q}_0 = \frac{1}{2}\vec{q}_L$	All branches $\frac{1}{2}\vec{q}_L$
	Three-sublattice	$T_N = 2.8$ K	$\vec{q}_0 = \frac{2}{3}\vec{q}_L$	All branches $\frac{2}{3}\vec{q}_L$
	Two-sublattice	$T_N = 1.8$ K	$\vec{q}_0 = \vec{q}_L$	LO(L), TO(L) LA[a](L), TA[a](L)
EuTe	Two-sublattice	$T_N = 9.6$ K	$\vec{q}_0 = \vec{q}_L$	LO(L), TO(L) LA[a](L), TA[a](L)

[a] Forbidden in dipole approximation—allowed only through wave-vector-dependent processes.

The wave-vector-dependent susceptibility is evaluated using the exchange constants of Ref. 1, listed in Table II. The divergence in the susceptibility at $\vec{k}=0$ ($\vec{q}=\vec{q}_L$) is antiferromagnetic EuTe, is indicative of critical fluctuations near the transition ($\kappa=0$). In other europium chalcogenides, $\chi(\vec{q})$ shows divergences near $\vec{q}=0$ for ferromagnetic EuO and EuS and at $\vec{q}=0$, $\frac{1}{2}\vec{q}_L$, $\frac{2}{3}\vec{q}_L$, and $\vec{q}_L$ for EuSe, corresponding to the different magnetic phases (see Table III).

In order to obtain an analytic expression for $I(T)$, we note that for $\hbar\omega_{LO} \gg k_B T$ the temperature dependence of the spectrum is governed mainly by the susceptibility, which has large variations with temperature for $\vec{q}=0$ for the ferromagnets and $\vec{k}=0$ for the antiferromagnets. We, therefore, expand the integrand of Eq. (38) around these wave vectors. The integrals over $\vec{q}$ and $\vec{k}$ are then evaluated using a spherical zone centered at Γ and L for the ferromagnet and antiferromagnet, respectively. To examine the dependence of the intensity on the correlation length, we define $I(\kappa) = I(T)/(T/T_c)$. For $T > T_c$, in the small wave-vector approximation,

$$I(\kappa) = I_F \frac{\kappa_0^2}{\nu_0} \int_0^{q_0} \frac{(\frac{1}{2}aq)^2 q^2 a q}{\kappa^2 + q^2} \tag{45}$$

for the ferromagnet and

$$I(\kappa) = I_A \frac{\kappa_0^2}{\nu_0} \int_0^{k_0} \frac{q^2 dq}{\kappa^2 + q^2} \tag{46}$$

for the two-sublattice antiferromagnet. In Eqs. (45) and (46), I_A and I_F are constants which are proportional to $|\beta+\gamma|^2$ defined in Eq. (29a), while ν_0 is the volume of the first Brillouin zone for the fcc lattice. The momentum cutoff in the integrals, q_0 (ferromagnet) and k_0 (antiferromagnet) corresponds to the radius of a sphere with volume ν_0 and $\frac{1}{4}\nu_0$ for the ferromagnet and antiferromagnet, respectively. The extra factor of q^2 in the expression for the ferromagnet is due to the vanishing of the Raman tensor at the Γ point. This factor results in a weaker temperature dependence of $I(T)$ for the ferromagnet than for the antiferromagnet, where the Raman tensor is a maximum in the region of large fluctuations.

Even though the integrated intensity does not diverge at T_c due to the phase-space and Raman-tensor factors, one can see that the small-wavelength (small k for the antiferromagnet) fluctuations are responsible for the temperature dependence of $I(T)$ if one differentiates Eqs. (45) and (46) with respect to κ. For the ferromagnet, $\partial I(\kappa)/\partial\kappa$ approaches 0 as $\kappa \to 0$, indicating that very near T_c, $I(0) - I(\kappa)$ varies quadratically with κ, while for the antiferromagnet, $\partial I(\kappa)/\partial\kappa \to$ constant as $\kappa \to 0$, implying that near T_c, $I(0) - I(\kappa)$ varies linearly with κ. The results of the integration of Eqs. (45) and (46), valid for the entire temperature range above T_c, in the small wave-vector approximation, are for the antiferromagnet,

$$I(\kappa) = I(0)\left[1 - \frac{\kappa}{k_0}\tan^{-1}\frac{k_0}{\kappa}\right], \tag{47}$$

and for the ferromagnet

$$I(\kappa) = I(0)\left[1 - 3\left(\frac{\kappa}{q_0}\right)^2 + 3\left(\frac{\kappa}{q_0}\right)^3 \tan^{-1}\frac{q_0}{\kappa}\right]. \tag{48}$$

For $T < T_c$, but $(T_c - T)/T_c$ small, one can use the cubic symmetry to write the integrated intensity in this region, $I^<(T)$, as

$$I^<(T) = \sum_{\substack{\vec{q},\sigma \\ j=1,0}} f_{isjs\sigma\sigma}(\vec{q}, \omega_i) \times\left[\frac{1}{3}\frac{\chi_\parallel(\vec{q})}{\chi_0} + \frac{2}{3}\frac{\chi_\perp(\vec{q})}{\chi_0}\right]\frac{S(S+1)}{3}, \tag{49}$$

where $\parallel$ and $\perp$ are taken relative to the direction of the spontaneous magnetization. In this temperature region,

$$\frac{\chi_\perp(\vec{q})}{\chi_0} = \frac{T/T_c}{g(\vec{q})}, \tag{50a}$$

$$\frac{\chi_\parallel(\vec{q})}{\chi_0} = \frac{(T/T_c)\kappa_0^2}{\kappa'^2 + g(\vec{q})\kappa_0^2}, \tag{50b}$$

where

$$\kappa'^2 = 2\kappa_0^2\left(\frac{T_c - T}{T_c}\right)^{2\nu'} \tag{51}$$

Mean-field theory gives $\nu' = \frac{1}{2}$. Similar expressions apply to the antiferromagnet, with $\vec{q}$ being replaced by $\vec{k} = \vec{q}_L - \vec{q}$ and with κ_0 defined by Eq. (43). Applying the small-wave-vector integration scheme to these expressions yields

$$I^<(\kappa') = \tfrac{1}{3} I(\kappa') + \tfrac{2}{3} I(0),$$

where $I(\kappa')$ is obtained from Eqs. (47) and (48) with κ replaced by κ'.

The analytic expressions for the broadline intensity show that the integrated intensity is parametrized by the ratio of the two basic lengths in the problem: κ^{-1}, which is the distance over which the spins are correlated, and q_0^{-1} (or k_0^{-1} for the antiferromagnet) which describes the range of wave vectors participating in the phonon-spin process. In a first approximation, q_0 or k_0 can be taken as the radius of a sphere surrounding the integration volume. However, since the small wave-vector approximation overestimates the Raman tensor for both the ferromagnetic and antiferromagnetic cases, one should adjust q_0 and k_0 to compensate for these errors. One therefore allows q_0 and k_0 to be adjustable parameters, de-

scribing the effective radius of the integration sphere, in order to enhance the validity of the small-wave-vector approximation away from $\kappa = 0$.

We have determined q_0 and k_0 by comparing $I(T_c)/I(\infty)$ using both the analytical expressions presented here and the same quantity calculated using the numerical integration scheme described above. Comparison of the numerical and analytical results suggest that we use the values

$$q_0/(\tfrac{3}{4}\nu_0/\pi)^{1/3} = 0.65, 0.73 \tag{52a}$$

for EuO and EuS, respectively, and

$$k_0/(\tfrac{3}{16}\nu_0/\pi)^{1/3} = 0.65 \tag{52b}$$

for antiferromagnet EuTe. Using these values in Eqs. (47) and (48), along with $\nu = \nu' = \frac{1}{2}$, we obtain results differing from those obtained by the numerical integration by <3%. Figure 2 shows our results for $I(T)/I(\infty)$ calculated using Eqs. (47), (48), and (52). Since the critical scattering is linear in κ near T_c for EuTe, the temperature derivative of $I(T)$ diverges like $(T - T_c)^{\nu-1}$, yielding the correlation length exponent ν. In all the materials the integrated intensity is a maximum at T_c due to the critical fluctuations. EuTe and EuSe, which exhibit two sublattice antiferromagnetic phases, show large increases in the integrated intensity near T_c due to the heavy weighting of the large fluctuations of $\chi(\vec{q}_L)$ in $I(T)$. On the other hand, EuO and EuS show only slight increases in the integrated intensity near T_c, corresponding to the small phase space and form-factor weighting of the small-$\vec{q}$ fluctuations which go critical in these materials. In EuS there is an additional contribution to the scattering from $\chi(\vec{q}_L)$ which increases near T_c due to the next-nearest-neighbor antiferromagnetic coupling in this material.

In addition to the temperature dependence of the integrated intensity, we have calculated the temperature dependence of the centroid of the spectrum $\langle\omega_{LO}\rangle_T$ using the numerical integration scheme described above and Eq. (39). Figure 3 shows the results of these calculations in a plot of $\langle\omega_{LO}\rangle_T/\langle\omega_{LO}\rangle_\infty$ vs T/T_c, where $kT \ll \hbar\omega_{LO}$. For EuS and EuO $\langle\omega_{LO}\rangle_T$ shows a small increase near T_c due to the increasing importance of the small-$\vec{q}$ phonons. On the other hand, there is a dramatic shift in $\langle\omega_{LO}\rangle_{T\to T_c}$ for EuSe where critical scattering at $H = 0$ is associated with $\pm\frac{1}{2}\vec{q}_L$, implying an increase in $\langle\omega_{LO}\rangle_T$. In all cases, away from T_c, $\langle\omega_{LO}\rangle$ is within 1% of the assumed L-point frequency, in accordance with the experiments of Ref. 8.

3. *Low temperatures ($T \ll T_c$)*

At low temperatures ($T \ll T_c$), the broadline scattering can be interpreted in terms of one-phonon–one-magnon scattering. Although the broadline is quenched as T is lowered below the transition temperature due to increasing spin order, there is residual broadline scattering even at $T = 0$ due to the scattering from creation of one phonon and one magnon. [For $k_B T \ll \hbar\omega_{LO}$ the ratio $I(0)/I(\infty)$ is $1/(S+1)$.] In addition, the second term of Eq. (31), the "Bragg peaks," begin to dominate the spectrum, yielding sharplines at the phonon frequency corresponding to the $\vec{q}$ vector which describes the magnetic order. Table III lists the types of ordering and the one-phonon–one-spin "Bragg reflected," dipole allowed phonons in all the europium chalco-

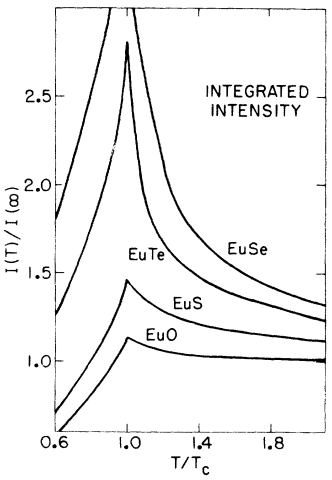

FIG. 2. Integrated intensity for zz-polarized one-phonon–one-spin Raman spectrum of europium chalcogenides as a function of T/T_c. The curves for each material are indicated in the figure.

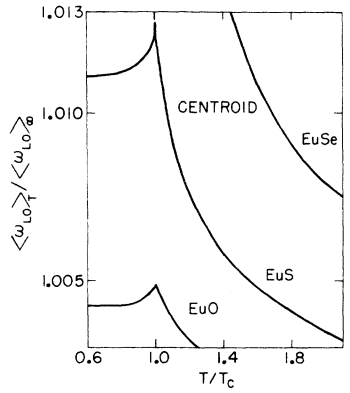

FIG. 3. Normalized centroid $\langle\omega\rangle_T/\langle\omega\rangle_\infty$ of zz-polarized LO one-phonon–one-spin spectrum of europium chalcogenides as a function of T/T_c. The variation of the centroid in EuTe was less than 0.1% and is thus not shown. At $T = T_c$, $\langle\omega\rangle_{T_c}/\langle\omega\rangle_\infty = 1.026$ for EuSe. Brillouin-zone integrations of Eq. (39) show that for $T \gg T_c$ but $T \ll \hbar\omega_{LO}/k_B$, $\langle\omega_{LO}\rangle$ (in cm^{-1}) is 413, 242, 155, and 132 for EuO, EuS, EuSe, and EuTe, respectively, using the values of Table II.

genides.[29] The contribution of the Bragg term of Eq. (31), nonzero for a single $\omega_{LO}(\vec{q})$ value in each magnetic phases, and which is elastic in $\omega - \omega_{LO}(\vec{q})$, results in the sharplines observed in the low-temperature, ordered phases of these materials.[9,10] These lines, previously interpreted in terms of zone folding,[29] can also be understood in terms of Bragg reflections of phonons by the spin systems, with the scattering intensities proportional to the square of the sublattice magnetization.[4] The assignment of the critical scattering above T_N, and the sharplines observed below T_N, observed in the four-sublattice phase of EuSe, to midzone $(\frac{1}{2}\vec{q}_L)$ phonons,[10] is consistent with Bragg scattering due to one-phonon–one-spin mechanism in this material. A mechanism quadratic in the spin, would result in sharpline scattering at the L-point phonons as well, which is not experimentally observed.[10] In addition, both broadline and sharpline scattering have been observed in *symmetric* polarizations,[10] consistent with the theory outlined above. An investigation of the field and temperature dependence of the broadline should yield information about the diffuse part of the two-spin correlation function, while a similar study of the sharpline scattering (off-resonance, symmetric polarization) can be used to measure the field and temperature dependence of the *sublattice* magnetization. However, sharpline scattering from the zone-center optic phonons is forbidden in the dipole approximation. The intensity of these lines depends on resonant enhancement[11] which decreases the convergence of the perturbation expansion in powers of the spin.

IV. DISCUSSION

A. Comparison with experiment

Although several discussions of the experimental data have suggested spin-disorder mechanisms, our analysis shows that both static and dynamic spin disorder must be considered in our evaluation of Eq. (27). The Raman line shape cannot be simply related to the one-phonon density of states, since the (full) width of the spectral weight function for EuS is approximately 10 cm^{-1} near $\vec{q}_L$, at high temperatures. The total broadline width calculated here is about 15 cm^{-1}, while the experimental results for EuS indicate a linewidth of about 30 cm^{-1}.[25] The full width of the broadline obtained from a δ function approximation for $F(\vec{q}, \omega)$ is less than 5 cm^{-1}, indicating the importance of including the $\vec{q}$ and exchange-dependent spectral weight function. The 15 cm^{-1} width calculated using Eq. (35), is a function of the simplified Raman-tensor parameters used in our calculations. A different choice of the parameters would allow more phonons to contribute and hence broaden the line. We have therefore presented the results for the temperature dependence (near T_c) of the moments of the spectrum, which are less sensitive to the assumed phonon dispersion, and which depend only on the static properties of the spins for $\omega_{LO} \gg k_B T/\hbar$.

However, in order to make contact with the existing experimental data,[7,30] we have considered the temperature dependence of the broadline peak. For zz polarization, we have shown that the Δ axis does not contribute to the spin-phonon spectrum, and that the peak of the broadline is near $\omega(\vec{q}_L)$, (see Fig. 3) consistent with the experimental results of Ref. 8. Assuming this peak to be dominated by the contribution of $\vec{q}_L$ implies that we can write the dynamic structure factor at the peak $[\omega = \omega_{LO}(\vec{q}_L)]$ as

$$\mathcal{S}(0, \omega_{LO}(\vec{q}_L)) \propto F(\vec{q}_L, 0)\chi(\vec{q}_L)/\chi_0 . \tag{53}$$

Since $F(\vec{q}, \omega)$ has unit area [see Eq. (33)], the peak of the spectral shape function can be approximated by the inverse of its width or characteristic frequency[1,31,34] which determines the linewidth in a neutron scattering experiment. By using the experimental values of the broadline peak intensity for $\mathcal{S}(0, \omega_{LO}(\vec{q}_L))$, and using the known temperature dependence of the susceptibility [in mean-field theory as in Eq. (32)], we can infer the temperature dependence of the characteristic frequency at $\vec{q}_L$. Figure 4 shows the unpolarized experimental data of Ref. 30 for the peak intensity of the broadline of EuS, along with mean-field calculations of $\chi(\vec{q})/\chi_0$ and the inferred characteristic frequency $\Gamma(\vec{q}_L)$ at the L point normalized to its value at T_c. Although spin-diffusion theory, valid at small values of $\vec{q}$ and ω, indicates that $\Gamma(\vec{q}_L)$, which is proportional to the diffusion constant, vanishes as the critical temperature is approached corresponding to the critical slowing down of fluctuations,[1,31,32] the detailed calculations of Hubbard[3] for the dynamics of spins in a simple cubic ferromagnetic show that the characteristic frequency or width increases as $T \to T_c^+$ for large wave vectors. This is shown in Fig. 4 where Hubbard's results for the width $[\delta_{\vec{q}_L}^{+}$ in the notation of Ref. 3] are plotted. The increase in $\Gamma(\vec{q}_L)$ as $T \to T_c^+$, indicated by our comparison of the experiments with Eq. (53), is also consistent with an extrapolation to large $\vec{q}$ of the predictions of dynamical scaling.[1,31,32] These arguments predict an increase in the linewidth in the region $q > \kappa$, where κ is the inverse correlation length (see Fig. 4). This prediction is corroborated by the neutron scattering results of Ref. 1, which have been fit to the (small-q) calculations of Resibois and Piette[32] for the width. These calculations show a minimum in the width $[\omega_\kappa(\vec{q})]$ as a function

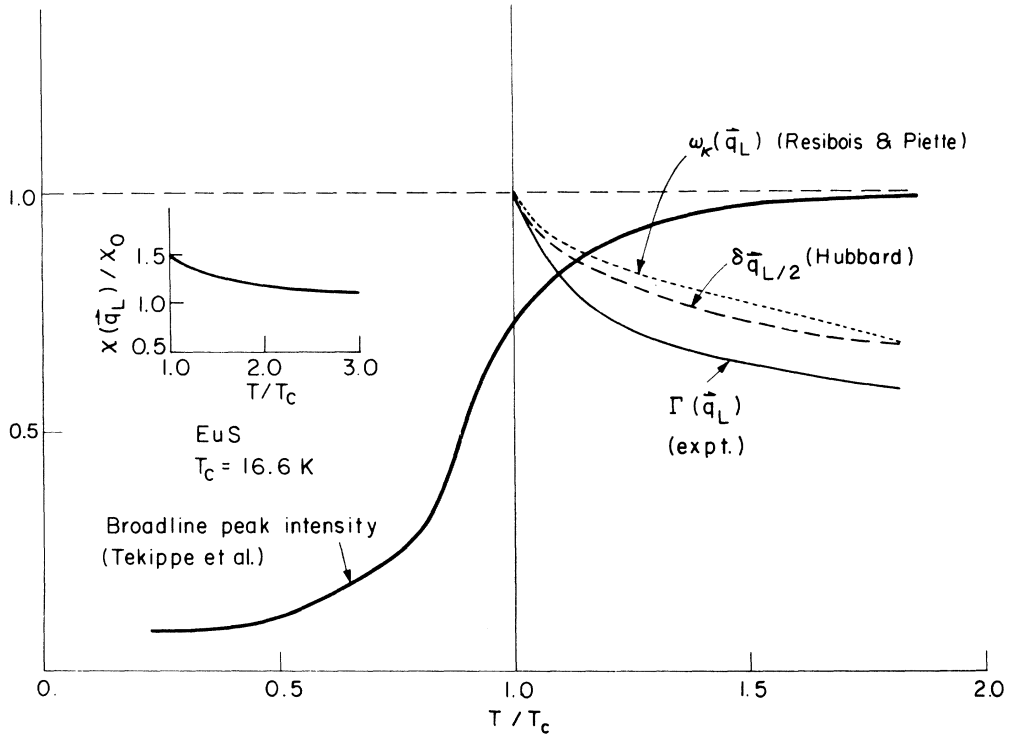

FIG. 4. Experimental results of Ref. 30 for the broadline peak intensity as a function of T/T_c. Using this data and Eq. (40), we have inferred the temperature dependence of the width of the spectral shape function $\Gamma(\vec{q}_L)$. In addition to $\Gamma(\vec{q}_L)$, we have also plotted the theoretical results of Ref. 32 for $\omega_\kappa(\vec{q}_L)$, the width of $F(\vec{q}_L,\omega)$, as a function of the correlation length κ, defined in Eq. (54). The dashed line represents the results of Hubbard (Ref. 3) for the halfwidth at $\vec{q} = \frac{1}{2}\vec{q}_L$. All the widths have been normalized to their values at T_c.

of κ at $q/\kappa \simeq 1$. Figure 4 presents the results for $\omega_\kappa(\vec{q})$, extrapolated to $\vec{q} = \vec{q}_L$. For EuS, the neutron experiments indicate that κ is given by

$$a\kappa \approx 3.30[(T - T_c)/T_c]^{0.7} , \tag{54}$$

so that for EuS, $\kappa/q_L = 1$ at about 50 K. Thus, the Raman experiments performed below this temperature are in the so-called critical regime,[31,32] where the hydrodynamic prediction of critical slowing down of fluctuations is invalid. Even though the inference of the temperature dependence of $\Gamma(\vec{q}_L)$ is based on unpolarized experimental data, it indicates how the one-phonon–one-spin Raman spectrum is sensitive to the spin dynamics in the europium chalcogenides.

Although our assignments of the broadline peak and the sharplines in EuSe are consistent with experiment,[8,10] more detailed measurements of the scattering (integrated) intensity as a function of temperature should further substantiate the theory presented here. We note that due to critical scattering at $\frac{1}{2}\vec{q}_L$ in the two-sublattice antiferromagnets EuTe and EuSe, and at $\frac{1}{4}\vec{q}_L$ in the four-sublattice phase of EuSe, the quenching of the broadline might not always be apparent since in the former cases the sharpline emerges at the same frequency as the broadline peak. In addition, in EuO, the combination of broadline scattering centered at the L point, and wave-vector-dependent resonant Raman scattering centered at the Γ point[11] might be difficult to separate[30] due to relatively flat dispersion along the [111] axis in this material.[8]

B. Comparison with other calculations

The results presented here indicate that at temperatures $\hbar\omega_{LO} \gg k_B T$ the temperature dependence of the Raman spectra is determined by the two-spin correlation function, which also governs the results of neutron scattering experiments. The similarity between Eq. (27) and the Van Hove formula [Eqs. (1) and (2) of Ref. 33] for neutron scattering suggests an analogy between the two spectra. In both cases, the cross section is proportional to the product of a form factor, describing the symmetry of the scattering, and the $(\vec{q},\omega)$ Fourier transform of the spin-spin correlation function. In the case of neutron scattering, the form factor for momentum transfer $\vec{K}$ is[33]

$$|F(\vec{K})|^2(\delta_{\alpha\beta} - K_\alpha K_\beta/K^2) ,$$

[where $F(\vec{K})$ is the atomic form factor], while for spin-dependent Raman scattering from phonons of wave vector $\vec{q}$, it is $f_{isj\sigma\sigma'}(\vec{q}, \omega_i)$ defined in Eq. (28). However, in neutron scattering from localized spins, the observed spectrum results from the direct dipole-dipole interaction of the neutron and atomic spins. The one-phonon–one-spin scattering discussed here, utilized an indirect coupling of the phonons and the spins through the electrons which are excited by radiation. In addition, the observed broadline spectrum consists of the sum of lines from $\vec{q}$ vectors from the entire zone. A line centered at a particular $\vec{q}$ vector has the same behavior as a function of temperature as would a line arising from a neutron scattering experiment where a neutron of momentum loss of $\vec{q}$ is used to probe a spin excitation. The similarity of the two spectra suggests an interesting physical interpretation of the spin-phonon scattering. The many-body phonon system, originally in a net zero-momentum state, is indirectly excited by the radiation to a superposition of excited states. The excited phonons in each of these states with momentum $\vec{q}$ can be viewed as probes of spin excitations of wave vector $-\vec{q}$, with the complication that phonons of all momenta (and all branches) are excited simultaneously in contrast to the selective excitation possible with neutrons.

The interpretation of the symmetrically polarized Raman scattering in the europium chalcogenides in terms of two-spin correlation functions, and the analogy with neutron scattering differs from the results obtained by Suzuki and Sakai and Tachiki in their treatments of broadline scattering in EuS.[16,17] Suzuki, arguing that the observed scattering has a symmetric component, rejects the one-phonon–one-spin mechanism on the grounds that it yields antisymmetric scattering. He thus interprets the broadline in terms of a four-spin correlation function. The complexity of this function leads to its evaluation by Suzuki in the infinite-temperature limit in the paramagnetic phases in contrast to our analysis of the $\vec{q}$ and T dependence of the two-spin correlation function for all the europium chalcogenides. Although Sakai and Tachiki do consider the one-phonon–one-spin process, they related only the antisymmetric component of the scattering to this process. The one-phonon–one-spin scattering can be seen to be *symmetric* if one considers the time-reversal properties of the spins, electric fields, and the non-zone-center phonons. When this is done, the selection rules listed in Table I are obtained, enabling the interpretation of both the parallel and perpendicularly polarized scattering in terms of two-spin correlation functions. In addition, the physical mechanism responsible for the one-phonon–one-spin process is spin-orbit coupling in the excited $4f^6 5d$ configuration. This coupling is large ($\simeq 0.6$ eV) in these materials,[34,35] resulting in a spin-dependent magnetoreflectivity spectrum.[36,10] On the other hand, the one-phonon–two-spin mechanism discussed by Suzuki is estimated to be weaker ($\simeq 0.05$ eV) than the spin-orbit energy.[16,17] Furthermore, any antisymmetric scattering process is reduced, off resonance, by a factor related to time reversal[37] [see Eq. (A8)].

C. Conclusion

In conclusion, we have derived a general method for determining the symmetry of the light scattering tensor under the interchange of the incident and scattered photon polarizations. This method has been applied to spin-phonon Raman scattering in the europium chalcogenides, where the fortuitous combination of inversion symmetry and large excited-state spin-orbit coupling enables the interpretation of the spectra in terms of the two-spin correlation function. At high temperatures ($T \gg T_c$), where there is complete static spin disorder, the broadline spectrum has been calculated assuming a Gaussian form describing the dynamical spin disorder. In the critical region ($T \approx T_c$), mean-field calculations of the wave-vector-dependent susceptibility have been used to calculate the temperature dependence of the broadline integrated intensity, related to static spin disorder. Our analytical results show how the integrated intensity can be used to study the temperature dependence of the correlation length. The sharplines observed in the ordered magnetic phases of the europium chalcogenides have been interpreted in terms of the elastic "Bragg" part of the two-spin correlation function. This unified analysis of the scattering in all the magnetic phases should stimulate further experiments in this area with an emphasis on using the excited phonons as probes to measure the static and dynamic properties of the model magnetic systems found in these materials.

Note added in proof. Calculations of the Raman integrated intensity using normalized Ornstein-Zernicke and renormalization-group forms for $\chi(\vec{q})$ indicate that $I(T)$ decreases near T_c for EuO and EuS. This is in contrast to the peaks predicted by mean-field theory as in Fig. 2. [S. Safran, Ph.D. Thesis (M.I.T. 1978) (unpublished)].

ACKNOWLEDGMENTS

We wish to thank Professor M. S. Dresselhaus, R. P. Silberstein, and L. E. Schmutz for useful discussions. We also wish to thank G. Gilat for making his integration program available to us.

APPENDIX

In this Appendix, we present an alternate derivation of the results of Sec. II B by explicit consideration of the matrix elements involved in one-phonon–one-spin scattering. Neglecting the spin energies ($\lesssim 10\ \mathrm{cm}^{-1}$) relative to the phonon energies, the Raman tensor for the one-phonon–one-spin process [Eq. (14)], can be written in the dipole approximation as[39]

$$\chi_{isj\sigma}(\omega_i, \omega_p, \vec{q}) = \sum_{\alpha\beta\gamma} [M^{\alpha\beta\gamma}_{i\sigma js}(0, 0, \omega_p, \vec{q}) + M^{\alpha\beta\gamma}_{ij\sigma s}(0, \omega_p, \omega_p, \vec{q}) + \cdots] . \quad \text{(A1)}$$

The dots in Eq. (A1) represent the contributions of the remaining terms in the perturbation expansion. The two terms shown are the largest and are written in terms of matrix elements as

$$M^{\alpha\beta\gamma}_{i\sigma js}(\omega_1, \omega_2, \omega_3, \vec{q}) = \frac{\langle 0|j_s|\gamma\rangle\langle\gamma|V_j(\vec{q})|\beta\rangle\langle\beta|L_\sigma(-\vec{q})|\alpha\rangle\langle\alpha|j_i|0\rangle}{(\omega_\gamma - \omega_i + \omega_3)(\omega_\beta - \omega_i + \omega_2)(\omega_\alpha - \omega_i + \omega_1)} . \quad \text{(A2)}$$

In Eq. (A2) we have used the notation of Sec. I. We define $\hbar\omega_p$ as the phonon energy and $V_j(\vec{q})$ as the electron operator corresponding to the linear interaction of the electrons with a phonon $Q(\vec{q}j)$ through the deformation potential or Fröhlich interactions. The Fourier transform of the σ component of the electron angular momentum operator $L_\sigma(-\vec{q})$ enters Eq. (A2) through spin-orbit coupling. The electronic states are represented by $|\alpha\rangle$, $|\beta\rangle$, $|\gamma\rangle$, with state $|i\rangle$ having energy $\hbar\omega_i$ and with the ground state $|0\rangle$, taken as the zero of energy. The full expression for the Raman tensor in fourth-order perturbation theory consists of 24 terms. The terms shown in Eq. (A1) are the largest for photon energies in the range of the $4f^7 \rightarrow 4f^6 5d$ transition ($\simeq$2 eV). However, the symmetry considerations presented here apply to all the terms in the Raman tensor. For those other terms, the factor $\omega_p/(\omega_0 - \omega_i)$ in Eq. (A8) should be replaced by $\omega_p/(\omega_0 + \omega_i)$ leading to an even smaller ratio of antisymmetric to symmetric scattering.

Equation (24) and the invariance of the ground-state expectation values under inversion symmetry imply that for centrosymmetric materials (each atom at a center of inversion):

$$\sum_{\alpha\beta\gamma} M^{\alpha\beta\gamma}_{i\sigma js}(0, 0, \omega_p, \vec{q}) = -\sum_{\alpha\beta\gamma} M^{\alpha\beta\gamma}_{i\sigma js}(0, 0, \omega_p, -\vec{q}) . \quad \text{(A3)}$$

Time-reversal symmetry of each matrix element dictates that

$$M^{\alpha\beta\gamma}_{i\sigma js}(0, 0, \omega_p, \vec{q}) = -M^{\gamma\beta\alpha}_{sj\sigma i}(\omega_p, 0, 0, -\vec{q}) . \quad \text{(A4)}$$

The antisymmetric (symmetric) part of the scattering is given by

$$\chi^{A,S} = \tfrac{1}{2}[\chi_{isj\sigma}(\omega_i, \omega_p, \vec{q}) \mp \chi_{sij\sigma}(\omega_i, \omega_p, \vec{q})] . \quad \text{(A5)}$$

The minus sign is for χ^A. From Eqs. (A3) and (A4) we have the results that

$$\sum_{\alpha\beta\gamma} M^{\alpha\beta\gamma}_{i\sigma js}(0, 0, \omega_p, \vec{q}) = \sum_{\alpha\beta\gamma} M^{\alpha\beta\gamma}_{sj\sigma i}(\omega_p, 0, 0, \vec{q}) \quad \text{(A6a)}$$

and

$$\sum_{\alpha\beta\gamma} M^{\alpha\beta\gamma}_{ij\sigma s}(0, \omega_p, \omega_p, \vec{q}) = \sum_{\alpha\beta\gamma} M^{\alpha\beta\gamma}_{s\sigma ji}(\omega_p, \omega_p, 0, \vec{q}) . \quad \text{(A6b)}$$

We can therefore write the antisymmetric part of the scattering as

$$\chi^A = \frac{1}{2}\sum_{\alpha\beta\gamma} [M^{\alpha\beta\gamma}_{i\sigma js}(0, 0, \omega_p, \vec{q}) + M^{\alpha\beta\gamma}_{ij\sigma s}(0, \omega_p, \omega_p, \vec{q}) - M^{\alpha\beta\gamma}_{ij\sigma s}(\omega_p, 0, 0, \vec{q}) - M^{\alpha\beta\gamma}_{i\sigma js}(\omega_p, \omega_p, 0, \vec{q})] . \quad \text{(A7)}$$

χ^A goes to zero as ω_p goes to zero. χ^A is also zero if we limit ourselves to the most resonant term, where $|\alpha\rangle = |\beta\rangle = |\gamma\rangle$. The first nonzero term in an expansion around $\omega_p = 0$ is, in the approximation $\omega_\alpha \simeq \omega_\beta \simeq \omega_\gamma \simeq \omega_0$,

$$\chi^A \simeq \frac{1}{2}\sum_{\alpha\beta\gamma} [M^{\alpha\beta\gamma}_{i\sigma js}(0, 0, 0, \vec{q}) - M^{\alpha\beta\gamma}_{ij\sigma s}(0, 0, 0, \vec{q})] \frac{\omega_p}{\omega_0 - \omega_i} . \quad \text{(A8)}$$

The symmetric scattering is nonzero even in the limit $\omega_p \rightarrow 0$, and is given by

$$\chi^S = \frac{1}{2}\sum_{\alpha\beta\gamma} [M^{\alpha\beta\gamma}_{i\sigma js}(0, 0, 0, \vec{q}) + M^{\alpha\beta\gamma}_{ij\sigma s}(0, 0, 0, \vec{q})] . \quad \text{(A9)}$$

χ^S is thus larger than χ^A by at least a factor of $\omega_p/(\omega_0 - \omega_i)$. Since in the paramagnetic phase of the europium chalcogenides the $4f^6 5d$ level can be modeled by a distribution of levels with a width of about 0.8 eV,[34] we estimate that the symmetric scattering intensity is at least two orders of magnitude greater than that of the antisymmetric scattering from the one-phonon–one-spin mechanism even at the peak of the broad absorption band. Furthermore, even in the ordered phases where the broad absorption band becomes a multipeaked structure with a typical peak width of 0.1 eV,[34] the

first factor of Eq. (A8) further reduces the scattering intensity of the antisymmetric term. For the most resonant case, $|\alpha\rangle = |\beta\rangle = |\gamma\rangle$, the contribution to χ^A from the largest terms in the Raman tensor is zero.

Similar considerations can be applied to the other spin-phonon processes to derive the selection rules of Table I.

---

*Also at Physics Dept., Massachusetts Institute of Technology, Cambridge, Mass.

†Supported by NSF Grant No. DMR 73-02473-A01.

‡Supported by the NSF.

[1]L. Passell, O. W. Dietrich, and J. Als-Nielsen, Phys. Rev. B 14, 4897 (1976); J. Als-Nielsen, O. W. Dietrich, and L. Passell, Phys. Rev. B 14, 4908 (1976); O. W. Dietrich, J. Als-Nielsen, and L. Passell, Phys. Rev. B 14, 4923 (1976).

[2]S. H. Liu, Phys. Rev. B 13, 2979 (1976).

[3]J. Hubbard, J. Phys. C 4, 53 (1971).

[4]W. Marshall and R. D. Lowde, Rep. Prog. Phys. 31, 705 (1971).

[5]J. C. Tsang, M. S. Dresselhaus, R. L. Aggarwal, and T. B. Reed, Phys. Rev. B 9, 984, 997 (1974).

[6]A. Schlegel and P. Wachter, Solid State Commun. 13, 1865 (1973).

[7]J. Vitins and P. Wachter, Solid State Commun. 17, 911 (1975).

[8]P. Grünberg, G. Güntherodt, A. Frey, and W. Kress, International Conference on Magneto-Optics, Zurich Physica (Utr.) 89B, 225 (1977).

[9]R. P. Silberstein, L. E. Schmutz, V. J. Tekippe, M. S. Dresselhaus, and R. L. Aggarwal, Solid State Commun. 18, 1173 (1976).

[10]R. P. Silberstein, V. J. Tekippe, M. S. Dresselhaus, Phys. Rev. B 16, 2728 (1977) (preceding paper).

[11]S. A. Safran, G. Dresselhaus, M. S. Dresselhaus, and B. Lax, International Conference on Magneto-Optics, Zurich; Physica (Utr.) 89B, 229 (1977).

[12]P. A. Fleury and R. Loudon, Phys. Rev. 166, 514 (1968).

[13]R. Loudon, J. Phys. C 3, 872 (1970).

[14]W. J. Brya and P. M. Richards, Phys. Rev. B 9, 2244 (1974).

[15]D. L. Mills, A. A. Maradudin, and E. Burstein, Ann. Phys. (N.Y.) 56, 504 (1970).

[16]N. Suzuki, J. Phys. Soc. Jpn. 40, 1223 (1976).

[17]O. Sakai and M. Tachiki (unpublished).

[18]D. Marcuse, *Engineering Quantum Electrodynamics* (Harcourt, Brace and Ward, New York, 1970), p. 393.

[19]A. A. Maradudin, E. W. Montroll, G. H. Weiss, and I. P. Ipatova, *Theory of Lattice Dynamics in the Harmonic Approximation* (Academic, New York, 1971).

[20]R. Loudon, Proc. R. Soc. A 275, 218 (1963).

[21]R. Kubo, J. Phys. Soc. Jpn. 12, 570 (1957).

[22]J. Callaway, *Quantum Theory of the Solid State* (Academic, New York, 1976), p. 530.

[23]D. L. Portigal and E. Burstein, J. Phys. Chem. Solids 32, 603 (1971).

[24]G. Dresselhaus and M. S. Dresselhaus, *Optical Properties of Solids, International School of Physics-Enrico Fermi, Varenna* (Academic, New York, 1966), p. 202.

[25]G. Güntherodt, in *Proceedings of the Thirteenth International Conference on the Physics of Semiconductor*, edited by F. G. Fumi (Tipografia Marves, Italy, 1977), pp. 291–300.

[26]G. Gilat and L. Bohlin, Solid State Commun. 7, 1727 (1969).

[27]M. F. Collins and W. Marshall, Proc. Phys. Soc. 92, 390 (1967).

[28]P. G. Klemmens, Phys. Rev. 148, 845 (1966).

[29]S. A. Safran, B. Lax, and G. Dresselhaus, Solid State Commun. 19, 1217 (1976); 20, vii(E) (1976).

[30]V. J. Tekippe, R. P. Silberstein, M. S. Dresselhaus, and R. L. Aggarwal, Phys. Lett. A 49, 295 (1974).

[31]B. I. Halperin and P. R. Hohenberg, Phys. Rev. 177, 952 (1969).

[32]P. Resibois and C. Piette, Phys. Rev. Lett. 24, 514 (1970).

[33]L. Van Hove, Phys. Rev. 95, 294, 1374 (1954).

[34]P. Wachter, Crit. Rev. Solid State Sci. 3, 189 (1972).

[35]T. Kasuya, Crit. Rev. Solid State Sci. 3, 131 (1972).

[36]C. R. Pidgeon, J. Feinleib, W. J. Scouler, J. O. Dimmock, and T. B. Reed, IBM J. Res. Dev. 14, 309 (1970).

[37]T. Moriya, J. Phys. Soc. Jpn. 23, 490 (1967).

[38]L. E. Schmutz, M. S. thesis (M.I.T., 1975) (unpublished).

[39]J. B. Sokoloff, J. Phys. C 5, 2482 (1972).